

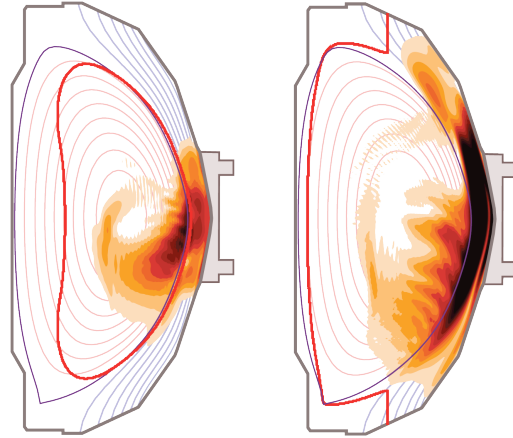
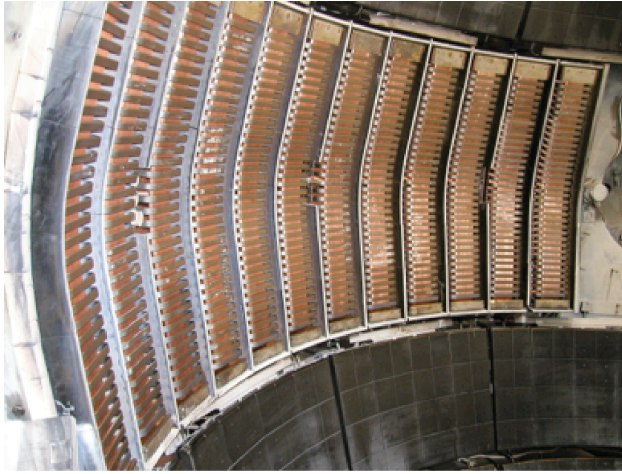
Table of Contents for Chapter 7

7.1 Overview of Goals and Plans.....	3
7.1.1 Introduction.....	3
7.1.2 Research Thrusts.....	7
7.1.2.1 Thrust RF-1: Develop of RF/EC Heating for Non-Inductive Plasma Current Start-Up and Ramp-Up.....	7
7.1.2.2 Thrust RF-2: Validate Advanced RF Codes for NSTX-U and Predict RF Performance in Future Devices.....	7
7.1.3 Research Needed to Enable Thrusts	8
7.1.3.1 Assess FW Interaction with Fast-Ions, and Develop Capability to Heat High-Power NBI H-Mode Plasmas with FW	8
7.1.3.2 Mitigation of FW Power Losses in the Scrape Off Layer.....	9
7.1.3.3 Model and Implement an EC/EBW Heating System.....	10
7.1.3.4 Develop Advanced Codes that Accurately Model RF Waves in NSTX-U	10
7.2 Research Plans for FW/EC Heating.....	10
7.2.1 FW Research Supporting Thrusts	11
7.2.1.1 Assess Performance of 12-Strap, Double-Feed FW Antenna and Compatibility with NBI H-Mode Discharges	11
7.2.1.2 Evaluate, Study and Mitigate RF Power Flows in the SOL and to the Divertors in the H-Mode Regime.....	11
7.2.1.3 Study FW Interaction with NBI Fast-Ions	12
7.2.1.4 Simulate/Mockup Reduced-Strap FW Antenna.....	13
7.2.1.5 Summary of Research Plan by Year for FW Research Supporting Thrusts	13
7.2.2 Thrust RF-1: Develop RF/EC Heating for Non-Inductive Plasma Current Start-Up and Ramp-Up	15
7.2.2.1 Fully Non-Inductive FW H-Mode, and Non-Inductive Plasma Current Ramp-up with FW Power	15
7.2.2.2 Assess Impact of FW Heating on NBI Current Ramp-up.....	16
7.2.2.3 EC Heating of CHI Plasma	16
7.2.2.4 Non-Inductive Start-up with EBW Heating.....	16
7.2.2.5 EBW Heating in NBI H-Mode Discharges.....	17
7.2.2.6 Summary of Research Plan by Year for Thrust RF-1	19
7.2.3 Thrust RF-2: Validate Advanced RF Codes for NSTX-U and Predict RF Performance in Future Devices.....	20
7.2.3.1 Validate Advanced RF Codes that Include SOL, Realistic Antenna Geometry, Accurate Modeling of Fast-Ion Interaction and the Effect of Edge Fluctuations....	20
7.2.3.2 Use of Advanced RF Codes to Predict RF Performance in ITER and Future Fusion Devices.....	21

NSTX Upgrade Research Plan for 2014-2018

7.2.3.3 Summary of Research Plan by Year for Thrust RF-2.....	21
7.3 Timelines for Tool Development Needed to Achieve Research Goals	22
7.3.1 Theory and Simulation Capabilities.....	22
7.3.1.1 AORSA Full-Wave Code.....	22
7.3.1.2 TORIC full Wave Code, with SOL Model	23
7.3.1.3 GENRAY Ray Tracing and TORBEAM Beam Tracing Codes	24
7.3.1.4 CQL3D Fokker-Planck Code.....	24
7.3.1.5 Diffusion Coefficient (DC) Code.....	26
7.3.1.6 AORSA/ORBIT-RF Full-Wave/Monte-Carlo Code	27
7.3.1.7 SPIRAL Using Fields from TORIC.....	28
7.3.1.8 Upgrade of NUBEAM with an RF Operator for FW.....	28
7.3.2 Diagnostics and Other Facility Upgrades Supporting Wave Heating and Current Drive Research.....	29
References.....	32

Chapter 7



Research Goals and Plans for Wave Heating and Current Drive

7.1 Overview of Goals and Plans

7.1.1 Introduction

Radiofrequency (RF) heating and current drive in both the ion and electron gyro-frequency regimes provide important tools that support the development of burning plasma science. Twenty megawatts of Ion-Cyclotron Range of Frequency (ICRF) heating are currently planned for the International Thermonuclear Experimental Reactor (ITER). Furthermore, Fusion Nuclear Science Facility (FNSF) designs based on the spherical torus (ST) do not have a central solenoid to drive the plasma current so the plasma needs to be initiated, ramped-up and sustained fully non-inductively. Fast wave (FW) power can, in principle, effectively ramp-up the plasma current through bulk plasma heating and bootstrap current enhancement in an FNSF ST device, even at low plasma currents where neutral beam current drive maybe ineffective due to poor fast-ion confinement. FW power is also a good candidate for on-axis non-inductive current generation in other future burning plasma devices. An FNSF ST device will operate in a plasma regime where the local electron plasma frequency can far exceed the electron cyclotron frequency. This “overdense” plasma regime precludes the use of conventional electron cyclotron heating (ECH) and electron cyclotron current drive (ECCD) to assist fully non-inductive plasma current ramp-

up and to suppress deleterious off-axis neoclassical tearing mode activity. In the overdense plasma regime electron Bernstein waves (EBWs) can provide efficient local electron heating and current drive with efficiencies that are better than the ECCD efficiencies achieved in “underdense” tokamak plasmas, and EBWs can efficiently drive current far from the magnetic axis [1, 2]. Note that in this chapter “Year 1” refers to the period covered by FY2014 and so on. There are two RF research thrusts for the period FY2014-18 that support high-level NSTX-U long-term goals noted in Chapter 1; high-level goal #1, to demonstrate stationary 100% non-inductive operation at performance levels that extrapolate to $\geq 1 \text{ MW/m}^2$ neutron loading in FNSF, is supported by thrust RF-1 (section 7.1.2.1), and high-level goal #3, to develop and understand non-inductive start-up/ramp-up in order to project to an FNSF ST, is supported by both thrusts RF-1 and RF-2 (section 7.1.2.2).

The FW antenna in NSTX-U will be essentially the same as the antenna used on NSTX,

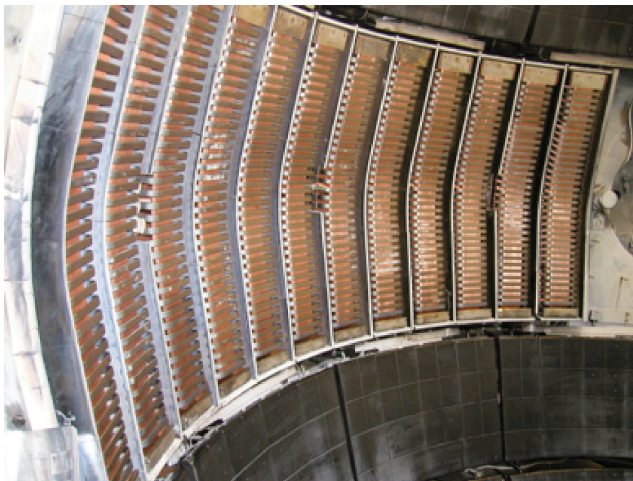


Figure 7.1.1: Photograph of the FW antenna in NSTX.

consisting of an array of twelve vertical current elements, or straps, driven by six 30-MHz transmitters. Figure 7.1.1 shows a photograph of the FW antenna viewed from inside the NSTX vacuum vessel. In front of each strap is a Faraday shield. The coupled power typically ranges from 1 to 4 MW, with up to 6 MW possible. The antenna extends toroidally 90 degrees around the vacuum vessel mid-plane. This is a flexible antenna system that is able to launch toroidally balanced (“heating phasing”) or directed (“current drive phasing”) wave spectra characterized by absolute values of parallel wavenumber, k_{\parallel} , between 3 and

18 m^{-1} , by adjusting the phase between adjacent antenna straps [3].

Traditional challenges for ICRF heating include achieving sufficiently high coupling from the antenna to the plasma in the good confinement region while simultaneously avoiding deleterious effects such as impurity release or overheating of plasma-facing components in the edge regions outside of the last closed flux surface (LCFS). A new loss mechanism was identified during high-harmonic FW (HHFW) experiments in NSTX: a major loss of RF power was sometimes observed to occur along open field lines passing in front of the antenna over the width of the scrape-off layer (SOL) [4-8]. In such cases, the heating efficiency was related to the location of the critical electron density (n_{ec}) for the onset of perpendicular FW propagation which is

proportional to $k_{\parallel}^2 \times B/\omega$, where B is the local magnetic field, and ω is the angular frequency of the wave. For 30 MHz FW heating of a discharge with $B_T(0) = 0.45$ T, at $k_{\parallel} = 8 \text{ m}^{-1}$ n_{ec} is $\sim 0.5 \times 10^{18} \text{ m}^{-3}$ and at $k_{\parallel} = 13 \text{ m}^{-1}$ n_{ec} is $\sim 1.6 \times 10^{18} \text{ m}^{-3}$. It is hypothesized that surface waves are being excited outside the radius where n_{ec} is located [4,5]. This hypothesis is supported by the observation that the flow of FW power is aligned along magnetic field lines that pass in front of the antenna throughout the radial width of the SOL [9]. If true, this suggests that this loss mechanism, distinct from the well-studied losses occurring directly at the antenna components, is common to various degrees in other ICRF heating systems. On NSTX-U, the increased magnetic field strength will enable greater exploration of the effects of the location of n_{ec} , while more detailed diagnostic measurements will confirm whether or not strong RF fields are present in the SOL. Further, SOL density control tools such as lithium coatings and divertor cryo-pumping will also influence the location of n_{ec} . These results will determine the validity of advanced numerical simulations of the RF power deposition in the SOL [10]. Fully understanding the underlying mechanisms behind this loss is critical for optimizing FW performance, and in particular for high-power, long-pulse ICRF heating in ITER.

Another issue of importance to ITER that can be addressed on NSTX-U is the assessment of the interaction of FWs with energetic ions generated by neutral beam injection (NBI). Results from NSTX-U experiments that heat neutral-beam-fuelled plasmas with FW power will be used to validate state-of-the-art RF simulation codes, that can in turn be used to predict the FW interaction with fast-ions in ITER, and other burning plasma devices. Since the toroidal field on NSTX-U can be operated at up to twice the level achieved on NSTX FW experiments in NSTX-U can be performed at lower ion cyclotron harmonics than was possible in NSTX. The lower harmonic ICRF heating in this medium-harmonic fast wave (MHFW) regime is expected to have less direct RF electron heating and significantly increased wave field interaction with ions, both thermal and NBI-generated fast-ions. Consequently at full field the FW system on NSTX-U will generate non-inductive current almost entirely via the bootstrap current that results from bulk plasma heating, rather than by a combination of bootstrap current and direct RF current drive. Due to the expense of using helium-3, ITER is considering FW heating of hydrogen for the “low-activation” phase, instead of using hydrogen discharges with a helium-3 minority. If this strategy is pursued on ITER the MHFW deuterium heating experiments on NSTX-U can provide important experimental data that is directly relevant to FW heating during the ITER “low-activation” phase.

FW experiments in NSTX have demonstrated that as little as 1.4 MW of FW power can generate and sustain an H-mode discharge with a plasma current of 300 kA and a non-inductive plasma current fraction of 0.7 – 1 [11]. FW experiments planned for NSTX-U will use much higher RF power and are predicted to demonstrate fully non-inductive plasma current ramp-up via bootstrap current overdrive. The results from NSTX-U FW experiments will be compared to predictions

from advanced RF numerical simulations. If the validity of the advanced RF codes can be validated for the NSTX-U FW experiments they will then be used to predict the FW performance in ITER and other burning plasma devices, such as a plasma-material-interface facility, FNSF and a Pilot Plant.

Non-inductive plasma start-up research will also benefit from the installation of a 1 MW 28 GHz EC/EBW heating system during the Year 3-4 timeframe. An upgraded version of this heating system, which has higher (≥ 2 MW) 28 GHz power and a steerable launcher, may later be used for off-axis EBW heating and current drive during the plasma current flat-top. An advanced microwave EBW imaging diagnostic will be deployed on NSTX-U in Year 2-3 to assess the EBW coupling efficiency in various NSTX-U plasma regimes. These emission measurements will provide important data that will guide the design of a multi-megawatt off-axis EBW heating and current drive system. To enable EBW heating the RF power is launched from external mirrors or waveguide arrays and is coupled to EBWs inside the overdense plasma via mode conversion in the SOL. EBW emission experiments on NSTX clearly demonstrated that the EBW mode conversion efficiency is significantly improved in the H-mode regime by using lithium wall conditioning to mitigate RF power losses in the SOL that occur as a result of collisions near the EBW mode conversion layer [12,13]. The EBW coupling efficiency increased from 10% to 60% when lithium conditioning was applied, and simulations predicted an increase from 30% to 80% due to the change in collisionality in the SOL. In NSTX-U at the higher toroidal field the electron temperature in the SOL will probably be higher than on NSTX so it is expected that the collisional EBW damping will be lower than on NSTX and the EBW coupling efficiency correspondingly higher. During the NSTX-U EBW emission experiments, lithium wall conditioning will be used to enhance the EBW mode conversion efficiency, and this will contribute to the experimental validation of advanced RF simulation codes that will be used to predict EBW heating performance in NSTX-U and future fusion research facilities. Longer-term, the effects of cryo-pumping on the SOL density and EBW emission, heating, and current drive will also be measured.

The remaining sub-sections of section 7.1 of this chapter provide an overview of the two major wave heating and current drive research thrusts and the research needed to support these thrusts. Section 7.2 presents detailed research plans. Section 7.3 reviews the timeline for tools that are needed to support the wave heating and current drive research plan; including theory and modeling requirements, plasma diagnostics, and NSTX-U facility upgrades. Schematic diagrams of the research and supporting tool implementation timelines are included at the end of this chapter. Research plans are presented for a baseline NSTX-U budget scenario and a scenario with a 10% incremental increase above the baseline budget.

7.1.2 Research Thrusts

As mentioned early, the 5-year plan for wave heating and current drive research on NSTX-U has two long-term research thrusts that are part of a long-range plan to support ITER, FNSF-ST, and other burning plasma research facilities. This section presents an overview of these research thrusts and some of the key research needed to support them.

7.1.2.1 Thrust RF-1: Develop of RF/EC Heating for Non-Inductive Plasma Current Start-Up and Ramp-Up

A major goal of the NSTX-U FY2014-18 research program is the development of fully non-inductive discharges that extrapolate to the neutron wall loading in FNSF, namely $\geq 1 \text{ MW/m}^2$. This goal is important for the design and development of future fusion research facilities. It is challenging both scientifically and operationally. The approach on NSTX-U will therefore be to initially develop non-inductive start-up, ramp-up and plasma sustainment scenarios separately, and then later combine these non-inductive scenarios. FW heating was successfully used in NSTX to generate a $> 70\%$ non-inductive H-mode discharge with a plasma current of $\sim 300 \text{ kA}$, using an inductively-initiated L-mode discharge as the target plasma for 1.4 MW of FW heating [11]. Three quarters of the non-inductive current in these NSTX experiments was bootstrap current and the remaining non-inductive current was generated directly by FW power. Modeling and experiments in NSTX-U will extend these FW H-mode studies by using much higher FW powers to demonstrate fully non-inductive plasma current ramp-up to plasma currents $\sim 500 \text{ kA}$. Coaxial Helicity Injection (CHI) was used for non-inductive start-up in NSTX, in NSTX-U high-power EC heating will be used to significantly increase the core electron temperature of CHI discharges in order to increase the plasma current and extend the non-inductive discharge duration to allow coupling of FW and NBI power. EBW heating will also be used to initiate plasma start-up in NSTX-U using a technique being developed on MAST [14]. More details of the NSTX-U non-inductive plasma formation and current ramp-up research plan are provided later in section 7.2.2 of this chapter and in chapter 8.

7.1.2.2 Thrust RF-2: Validate Advanced RF Codes for NSTX-U and Predict RF Performance in Future Devices

NSTX-U will operate with toroidal magnetic fields up to 1 T, nearly twice the value used during the experiments on NSTX. While the dominant RF heating mechanisms in the HHFW regime in NSTX were direct electron heating, via Landau damping and Transit Time Magnetic Pumping, and NBI fast-ion acceleration, in the MHFW regime in NSTX-U the power partitioning is expected to change. Simulations of NSTX-U discharges with the AORSA [15], TORIC [16] and GENRAY [17] numerical codes predict significantly more thermal deuterium damping in the

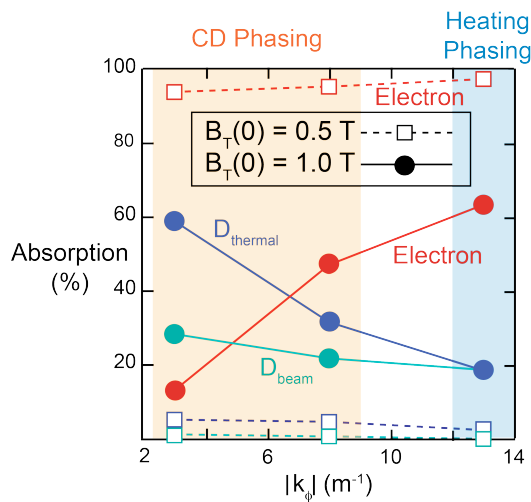


Figure 7.1.2: 30 MHz absorption versus launched wavenumber (k_{\parallel}) calculated by AORSA for a $B_T(0) = 1$ T, and a $B_T(0) = 0.5$ T NSTX-U NBI + FW deuterium H-mode discharge with $n_e(0) = 1.09 \times 10^{14} \text{ cm}^{-3}$, $T_e(0) = 1.22 \text{ keV}$, $T_i(0) = 2.86 \text{ keV}$. Strong RF absorption by thermal deuterium is predicted at the higher $B_T(0)$, especially at the smaller k_{\parallel} used for CD. Absorption by deuterium is predominantly at the fifth ion cyclotron harmonic. Plasma parameters obtained from TRANSP run 142301G90 at 7 s.

Planck neoclassical simulation code [18, 19]. These and other RF codes will be valuable tools for predicting the behavior of the wave fields in the SOL, the plasma edge, and the interaction with fast-ions in the bulk plasma in future burning plasma devices, including ITER. However the RF codes need to be validated against experimental data on present devices, such as NSTX-U. Accurate validation will require detailed measurements in the SOL, including edge fluctuations, RF power flows to the divertor regions, the RF power deposition profile and the current density profile. After these advanced RF simulation models have been validated during the first three years of this plan they will be used to predict RF performance in future burning plasma devices. More details of the advanced RF code validation plans are provided in section 7.2.3, and details of the RF codes are presented in section 7.3.1.

7.1.3 Research Needed to Enable Thrusts

7.1.3.1 Assess FW Interaction with Fast-Ions, and Develop Capability to Heat High-Power NBI H-Mode Plasmas with FW

A significant increase in neutron rate, and an enhancement and broadening of the fast-ion profile were measured in NBI-fuelled plasmas in NSTX when FW heating was applied [7]. These

higher magnetic fields in NSTX-U [Fig. 7.1.2]. The lower electron beta at the higher magnetic fields in NSTX-U will result in less direct electron absorption and as a result more FW power will accelerate NBI fast-ions and thermal ions than it did in NSTX, particularly when long-wavelength, “current drive”, antenna phasings are used. It is important to assess the heating and direct current drive capability of the FW system over a wide range of launched wavenumbers, toroidal magnetic fields, and electron densities in NSTX-U, and compare the experimental results to predictions by advanced RF numerical codes. These codes include the AORSA-3D full-wave solver [10] with SOL modeling and a realistic antenna model, and the full finite-orbit-width CQL3D Fokker-

observations indicated a strong interaction between FWs and NBI fast-ions. At the axial toroidal fields used on NSTX ($B_T(0) \leq 0.55$ T) there was often a significant loss of FW-accelerated NBI fast-ions from the plasma. Lithium conditioning enabled the first observation of significant FW central heating during NSTX NBI-fuelled deuterium H-mode plasmas, but when the NBI beam power was increased from 2 to 4 MW there was a noticeable increase in heating of the limiter surrounding the FW antenna, resulting from NBI fast-ion bombardment. A more robust limiter may be installed to protect the FW antenna from this fast-ion heating during Year 4 of the incremental plan. This upgraded limiter would provide better compatibility with the higher NBI powers available on NSTX-U. The need for a FW limiter upgrade will be assessed in Year 2-3. At the higher magnetic fields in NSTX-U the fast-ion interactions with the antenna should be reduced since the Larmor radius (and banana width at higher plasma current) will be smaller. Also the effect of the higher magnetic fields on the FW interaction with NBI fast-ions will be assessed on NSTX-U. During these experiments the FW interaction with NBI fast-ions generated by the new larger tangency radius neutral beam sources will be compared to the interaction with fast ions from the original neutral beam.

7.1.3.2 Mitigation of FW Power Losses in the Scrape Off Layer

FW heating and current-drive efficiencies on NSTX were significantly decreased by interactions of the FW power with the plasma in the SOL [4-8]. These SOL interactions result in RF power flowing from the antenna to the lower and upper divertor regions, where bright spirals are produced [Fig. 7.1.3]. The location of the spirals in the divertor regions is consistent with the hypothesis that FW power flows through the SOL to the divertor regions along magnetic field lines that pass in front of the antenna [9]. These results are important for benchmarking advanced RF codes, and for predicting the amount of FW power coupled to the SOL [10]. Fully understanding and mitigating the underlying mechanisms behind this power loss in NSTX-U is critical for optimizing FW performance in general. $B_T(0)$ and plasma current (I_p) in NSTX-U will be up to twice as high as in NSTX, which has several implications for FW coupling and heating efficiency in NSTX-U; higher B_T in NSTX-U moves the n_{ec} towards or inside the LCFS, reducing surface wave losses. The SOL width may shrink

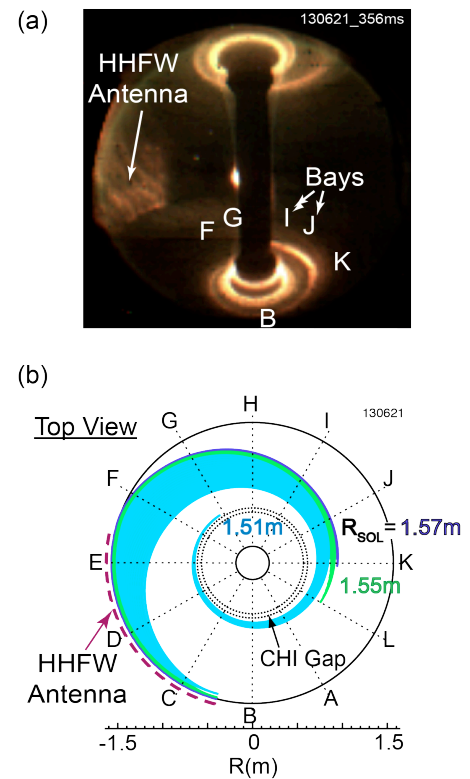


Figure 7.1.3: (a) Visible camera image of FW power flow to the divertor regions in NSTX during a $B_T(0) = 1$ T H-mode discharge with 1.4 MW of FW power and 2 MW of NBI power (shot 130621 at 356 ms). (b) SPIRAL modeling of SOL field lines from FW antenna to the divertor for the same discharge and time as (a).

at higher I_p , reducing surface wave losses. Also, the higher electron density during high-power NBI in NSTX-U may increase the SOL density moving n_{ec} outside the LCFS and closer to the wall, and possibly increasing surface wave losses. So experiments in Year 2-3 to understand and mitigate FW power loss in the SOL will involve modifying the SOL density profile with gas puffing, lithium conditioning, and by varying I_p and $B_T(0)$ to move n_{ec} . When the cryo-pump becomes available in Year 4 it can also be used to change the location of n_{ec} . Additional IR cameras and RF probes on NSTX-U will allow a better characterization of the FW power flow to the divertor and its toroidal heat deposition.

7.1.3.3 Model and Implement an EC/EBW Heating System

With baseline funding a 28 GHz 1 MW EC/EBW heating system will be installed in Year 4. Initially this system will provide electron heating during non-inductive plasma start-up, later it will be used for off-axis EBW heating and current drive. The CQL3D Fokker-Planck code [18, 19] applied to electrons has enabled calculation of EBW absorption and current drive in the NSTX tokamak. Similar scoping work and analysis will be carried out for NSTX-U for start-up heating scenarios and for off-axis heating and current drive during the plasma current flat top.

7.1.3.4 Develop Advanced Codes that Accurately Model RF Waves in NSTX-U

While significant progress has recently been made developing numerical codes that can accurately model RF power flows and deposition in the core, edge and SOL, currently advanced RF codes, such as the AORSA full-wave code [15], lack accurate antenna geometry. Also slow-wave propagation in the SOL is not accurately modeled due to resolution constraints and because the SOL density profiles used have been approximate due to the lack of SOL measurements. During Year 1-2 the SciDAC Center for Simulation of Wave-Particle Interactions (CSWPI) has milestones to add these more accurate, high-resolution antenna and SOL modeling capabilities to AORSA and the full-wave TORIC solver [16]. As these modeling enhancements become available they will be employed to support FW studies on NSTX-U.

7.2 Research Plans for FW/EC Heating

This section presents the plans for wave heating and current drive research. Section 7.2.1 covers FW research that supports both RF thrusts, section 7.2.2 covers research for thrust RF-1 and section 7.2.3 covers research for thrust RF-2. Sections 7.2.1.5, 7.2.2.6 and 7.2.3.3 contain bulleted, year-by-year summaries for these research plans. Note FY2014 is “Year 1” in the plans.

7.2.1 FW Research Supporting Thrusts

7.2.1.1 Assess Performance of 12-Strap, Double-Feed FW Antenna and Compatibility with NBI H-Mode Discharges

In April 2009, prior to bakeout of NSTX and the beginning of the 2009 experimental campaign, the single-feed, end-grounded FW antenna straps were replaced with double-feed, center-grounded straps to reduce RF electric fields in the vicinity of the Faraday shield for a given strap current. However, the installation of the transmission lines was not completed until July 2009, by which time approximately 300 g of lithium had been deposited in the machine, much of it on the antenna itself. After several days of plasma conditioning reliable high power operation (~ 4 MW) was obtained towards the end of the 2009 campaign, but the double-feed antenna performance was never evaluated during NBI H-mode discharges without prior lithium conditioning, or at least with minimal lithium conditioning [20]. For the 2010 experimental campaign some operational changes were made to accommodate the Liquid Lithium Divertor (LLD) that further degraded the FW antenna performance; there was no boronization of the machine, no glow discharge cleaning between plasma discharges, and increased lithium evaporation rates (typically a factor of two higher than during the 2009 campaign). Furthermore the LLD was prefilled before plasma operation. Consequently the maximum arc-free FW power coupled to the plasma in 2010 was less than 2 MW. For all these reasons the performance of the 12-strap, double-feed FW antenna configuration and its compatibility with NBI H-mode discharges will be assessed for a range of NBI powers during years 2-3 of the 5-year plan.

7.2.1.2 Evaluate, Study and Mitigate RF Power Flows in the SOL and to the Divertors in the H-Mode Regime

It is important to both evaluate the FW power flows through the SOL to the divertor regions in NSTX-U [9], and to explore strategies that can mitigate these power flows (eg. by using lithium conditioning and gas puffing to change the SOL density, and by adjusting the outer gap and plasma shape). The Langmuir probe sets in the divertor tiles will be augmented to include some that have direct RF detection capability. RF probes in the tiles above and below the antenna will be installed prior to the start of NSTX-U operations. These probes will allow the measurement of the relative strengths of the RF fields propagating in both directions (co and counter) along the magnetic field lines. A new wide-angle infra-red (IR) camera viewing the lower divertor and a fast IR camera with a narrower view of the upper divertor will be installed prior to the start of NSTX-U operations. These are in addition to the two existing IR cameras viewing the divertors. Both the new IR cameras are funded in the baseline budget. RF probes in the divertor tiles will directly measure RF power deposition and Langmuir probes will allow the FW field strength to be measured in the vicinity of the RF-produced spiral deposition region. RF magnetic field

strength and RF-induced currents in the vicinity of the RF-produced spirals will also be measured. Probes in the floor and ceiling of NSTX-U will measure the directionality of wave excitation and separate direct propagation effects from standing wave effects. Measurements from the four IR cameras and the RF probes will permit a more complete quantitative assessment of RF power flow patterns across the mid-plane SOL and in the divertor regions in order to validate advanced RF codes. The detailed evaluation of the RF power flows in the SOL will be performed in years 2-3 of the 5-year plan. The effect of the cryo-pump and 3-D fields on RF power flows in the SOL will be assessed in Years 4-5.

7.2.1.3 Study FW Interaction with NBI Fast-Ions

Experiments that combined FW and NBI heating in NSTX showed a competition between two dominant absorption mechanisms in the plasma, namely direct electron heating (via Landau damping and transit-time magnetic pumping) and wave-field acceleration of NBI generated fast-ions. While it was possible to achieve good FW electron heating in Ohmic NSTX target plasmas, this was not necessarily the case when NBI power was also applied. TORIC [16] calculations, based on experimental magnetic and kinetic measurements, revealed that a large fraction (~ 50%) of the power absorbed within the LCFS can be deposited on the fast-ions, at the expense of direct electron heating. This fast-ion heating was undesirable in part because these RF-accelerated particles were poorly confined in NSTX [21], and because it limited the RF power available for current drive by reducing the power transferred to the electrons. An implementation of TORIC into the TRANSP [22] analysis software was used to compute realistic time dependent FW power deposition in NSTX plasmas. It was found that the portion of FW power going to the fast-ions decreased with time as these particles were progressively thermalized [23] consistent with the observed time evolution of the neutron production rate during the FW heating pulse.

NSTX-U will expand the operational range of FW heating to lower ion cyclotron harmonics. In particular, the higher maximum magnetic field will move n_{ec} towards the LCFS and hence reduce losses originating in the SOL that were previously observed in NSTX [9]. Moreover the larger plasma current will better confine the RF-accelerated ions. It is also expected that thermal-ion heating by FWs will become appreciable at the higher magnetic field in NSTX-U. In addition to indirect observations mentioned above, the fast-ion D-alpha (FIDA) [24] diagnostic will provide time and spatially resolved information about the fast-ion density and acceleration, enabling a better understanding of the physics of the FW heating in the presence of NBI. These experiments will be conducted in collaboration with the NSTX-U Energetic Particles group to study the effect of FW heating on the spectrum of Alfvén eigenmode (*AE) activity and fast-ion transport (see section 6.3.3.4). Experimental studies of the FW interaction with NBI fast-ions will be performed in years 2-4 of the 5-year plan.

7.2.1.4 Simulate/Mockup Reduced-Strap FW Antenna

The baseline 5-year plan for the FW antenna is to reduce the number of current straps used for FW heating from 12 to 8 to make room available for antennas that will excite *AE modes and/or use some of the FW antenna straps to excite edge harmonic oscillations (EHOs) after Year 5 in the incremental plan. Before implementing any changes to the number of antenna straps experiments will evaluate the performance of the 12-strap FW antenna when it is configured with only eight active straps. These mocked up reduced-strap experiments will be performed in Year 5.

7.2.1.5 Summary of Research Plan by Year for FW Research Supporting Thrusts

Assuming a Baseline Funding Scenario (*Baseline + 10% incremental scenario in italics*)

Year 1 (FY2014):

- Complete simulation of FW heating during non-inductive I_p ramp-up and the I_p flat top.

Year 2:

- Assess performance of 12-strap, double-feed, FW antenna and its compatibility with NBI H-mode $B_T(0) \leq 0.8$ T discharges. Experiments will be performed with 2-3 MW of FW coupled power in a boronized machine, with the minimum lithium conditioning needed to achieve good FW coupling. Both heating and current drive antenna phasings will be used during these experiments. $B_T(0)$ will be scanned from 0.5 to 0.8 T. The amount of lithium conditioning will be increased to assess the performance of the FW antenna and the plasma heating efficiency.
- Evaluate, study and mitigate RF power flows in the SOL and to the divertor regions in the H-mode regime in $B_T(0) \leq 0.8$ T discharges. Experiments will be performed with 2-3 MW of FW coupled power and 2-4 MW of NBI power in a boronized machine with minimal lithium conditioning. $B_T(0)$ will be scanned from 0.5 to 0.8 T. Both heating and current drive antenna phasings will be used during these studies. Once the SOL RF power flows have been well characterized with RF probes, IR cameras etc., lithium conditioning, gas puffs and outer gap scans will be introduced in an attempt to mitigate the SOL RF power flows to the divertor regions.
- Study FW interaction with NBI fast-ions in $B_T(0) \leq 0.8$ T discharges. $B_T(0)$ will be increased from 0.5 to 0.8 T. The antenna phase will scanned at each level of $B_T(0)$ and a

comparison will be made between the interaction with fast-ions from the original beam lines and the new more tangential beam lines.

Year 3:

- Assess performance of 12-strap, double-feed, FW antenna and compatibility with NBI H-mode $B_T(0) \leq 1$ T discharges. Experiments will be performed with 3-5 MW of FW coupled power in a boronized machine, with the minimum lithium conditioning needed to achieve good FW coupling. Both heating and current drive antenna phasings will be used during these experiments. $B_T(0)$ will be scanned up to 1.0 T. The amount of lithium conditioning will be increased to assess the performance of the FW antenna and the plasma heating efficiency.
- Evaluate, study and mitigate RF power flows in the SOL and to the divertor regions in the H-mode regime in $B_T(0) \leq 1$ T discharges. Experiments will be performed with 3-4 MW of FW coupled power and 2-4 MW of NBI power in a boronized machine with minimal lithium conditioning. $B_T(0)$ will be scanned up to 1.0 T. Both heating and current drive antenna phasings [3] will be used during these studies.
- Continue to study FW interaction with NBI fast-ions in $B_T(0) \leq 0.8$ T discharges.
- *Study FW interaction with NBI fast-ions in $B_T(0) \leq 1$ T discharges. (see Year 4 for more details)*

Year 4:

- Study FW interaction with NBI fast-ions in $B_T(0) \leq 1$ T discharges. The antenna phase will scanned at each level of $B_T(0)$ and a comparison will be made between the interaction with fast-ions from the original beam lines and the new more tangential beam lines.
- *Assess the effect of cryo-pumping and 3-D fields on FW coupling. The cryo-pump and 3-D fields may help to mitigate RF losses in the SOL by lowering the SOL density.*
- *Reduced-strap FW antenna mockup experiments. (see Year 5 for more details)*

Year 5:

- Assess the effect of cryo-pumping and 3-D fields on FW coupling. The cryo-pump and 3-D fields may help to mitigate RF losses in the SOL by lowering the SOL density.
- Reduced-strap FW antenna mockup experiments. These experiments will test heating and current drive antenna phasing during the plasma current flat top of FW-only H-mode discharges, H-mode discharges that combine FW and NBI heating, and for FW-assisted non-inductive plasma current ramp-up. Before these experiments are conducted,

numerical simulations will be performed to determine the coupled spectra of modes for a range of antenna phasings and the resulting RF power deposition and current drive profiles in various NSTX-U target discharges.

7.2.2 Thrust RF-1: Develop RF/EC Heating for Non-Inductive Plasma Current Start-Up and Ramp-Up

This research thrust supports the research goals of the NSTX-U Solenoid Free Plasma Start-Up Topical Science Group (SFPS TSG), whose research plans and goals are discussed in detail in Chapter 8. Here we review experimental plans for non-inductive plasma current ramp-up and start-up that utilize FW, EC and EBW heating and current drive that support experiments also discussed in sections 8.6.3, 8.6.4 and 8.7.5.

7.2.2.1 Fully Non-Inductive FW H-Mode, and Non-Inductive Plasma Current Ramp-up with FW Power

In 2010 1.4 MW of $k_{||} = -8 \text{ m}^{-1}$ FW power (current drive antenna phasing) was coupled into an I_p

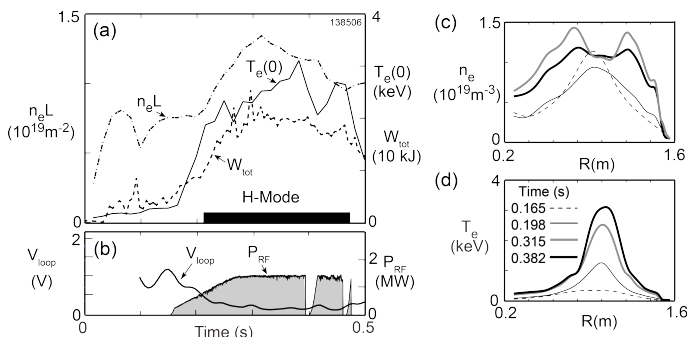


Figure 7.2.1: Time evolution of an $I_p = 300 \text{ kA}$ FW-generated H-mode plasma (shot 138506) that maintained good FW coupling to the core during the H-mode phase. (a) Line integrated density ($n_e L$), central electron temperature ($T_e(0)$) and total plasma stored energy (W_{tot}) versus time. (b) The time evolution of the measured loop voltage (V_{loop}) and RF power. (c) Electron density and (d) electron temperature versus major radius at four times during shot 138506; 0.165 s, (dashed line), 0.282 s (thin solid black line), 0.298 s (thick solid grey line) and 0.382 s (thick solid black line).

feedback between a high $T_e(0) \sim 3 \text{ keV}$, and a relatively high RF current drive efficiency $\sim 0.1 \text{ MA/MW}$. However, lithium compound dust in the antenna played a major role in limiting the arc-free FW power to $\sim 1.4 \text{ MW}$. While lithium conditioning has been found to be

$= 300 \text{ kA}$, $B_T(0) = 0.55 \text{ T}$ Ohmic target plasmas (XP-1009) generating a sustained H-mode and achieving a non-inductive current fraction, $f_{NI} = 0.7 - 1.1$. This result was the consequence of better plasma control, the improved RF coupling due to lithium conditioning, and the positive

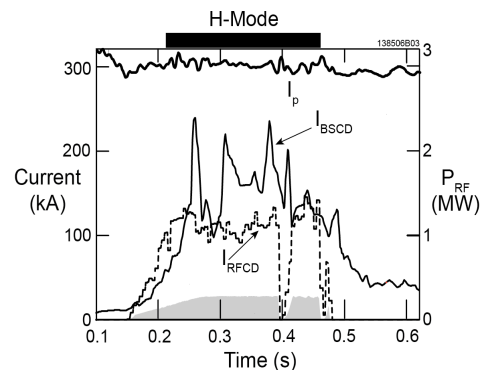


Figure 7.2.2: I_p (thick solid line), I_{BS} (thin solid line) and I_{FWCD} (dashed line) calculated by TRANSP-TORIC for shot 138506, and the RF power (Gray shading) plotted versus time.

generally beneficial for improving FW coupling in NSTX in the past [7], two vacuum leaks produced the dust after extensive lithium conditioning. Another issue with the experiments in 2010 was that NBI source A was not available to provide the heating neutral beam blips necessary for documenting the evolution of $q(R)$ and T_i . Figure 7.2.1 summarizes the results for the best discharge from XP-1009, shot 138506. An H-mode was generated soon after turn-on of the FW power that had good on-axis electron heating. Figure 7.2.2 shows TRANSP-TORIC modeling results for shot 138506, assuming 100% of the FW power is coupled to the discharge. The coupling efficiency was actually $\sim 60\%$ during this discharge, so only $\sim 25\%$ of the non-inductive current was driven directly by FW power, the rest is bootstrap current, which fluctuated by about 50% due to changes in the off-axis electron pressure. A more stable electron pressure profile is needed to control the magnitude of the non-inductive current. Fully non-inductive FW H-mode experiments will be performed in Years 2-3 of the 5-year plan.

7.2.2.2 Assess Impact of FW Heating on NBI Current Ramp-up

TSC simulations predict that starting from a 400 kA inductive target, bootstrap current overdrive and neutral beam current drive can ramp-up the plasma current to 1 MA in about 3 seconds. In these simulations, an initial 400 kA low-inductance discharge is heated using 4 MW of FW power. The H-mode is initiated at about 150 ms. The NBI power is programmed to increase with the plasma current. The FW power is turned off in the simulations at 900 ms to limit the NBI fast-ion interaction with the antenna. A combination of NBI and FW heating will be used to non-inductively ramp-up the plasma current from 300-400 kA to 0.8-1 MA during Years 3-4 of the 5-year plan. These experiments will assess the impact of adding FW heating to the NBI heated current ramp-up.

7.2.2.3 EC Heating of CHI Plasma

CHI-only target plasmas have $T_e(0) < 10$ eV and pulse lengths that are only 20-40 ms. EC heating at the megawatt-level will significantly increase $T_e(0)$ and the current persistence time. GENRAY [17] modeling of a NSTX CHI plasma with $B_T(0) \sim 0.5$ T (shot 148072) predicts $\sim 25\%$ first-pass absorption of 28 GHz X-mode EC power (see section 8.9.3). With baseline NSTX-U funding a megawatt-level, 28 GHz EC heating system is planned for installation on NSTX-U by Year 4. When the 28 GHz heating system has been commissioned into low density inductive plasmas and becomes available for experiments it will be used to heat CHI target plasmas.

7.2.2.4 Non-Inductive Start-Up with EBW Heating

EC heating cannot be used to heat start-up plasmas once the plasma density exceeds the critical density for EC wave propagation. In this so-called “overdense” regime EBW heating can be used

5 s, will heat electrons locally off-axis, and will also efficiently drive current off-axis via Ohkawa current drive (see ref. [1, 2] and references therein).

GENRAY ray tracing [17] and CQL3D Fokker-Planck modeling [18, 19] has been performed for EBW heating in a 1.1 MA advance scenario NSTX-U H-mode plasma with 6 MW of NBI heating, an axial toroidal field of 1 T (TRANSP run 142301V11 at 11.875 s). The density and temperature profiles used for the modeling are shown in Fig. 7.2.3(a). The electron cyclotron resonances and cutoffs for this plasma are shown in Fig. 7.2.3(b). 28 GHz EBWs are resonant with f_{ce} at $R \sim 0.95$ m, close to the magnetic axis. The O-X-B conversion efficiency was calculated as a function of poloidal and toroidal angle and the results are summarized in Fig. 7.2.4. The maximum O-X-B mode conversion efficiency was obtained for a poloidal angle of ± 10 degrees and a toroidal angle of ± 38 degrees, corresponding to $n_{\parallel} = \pm 0.7$.

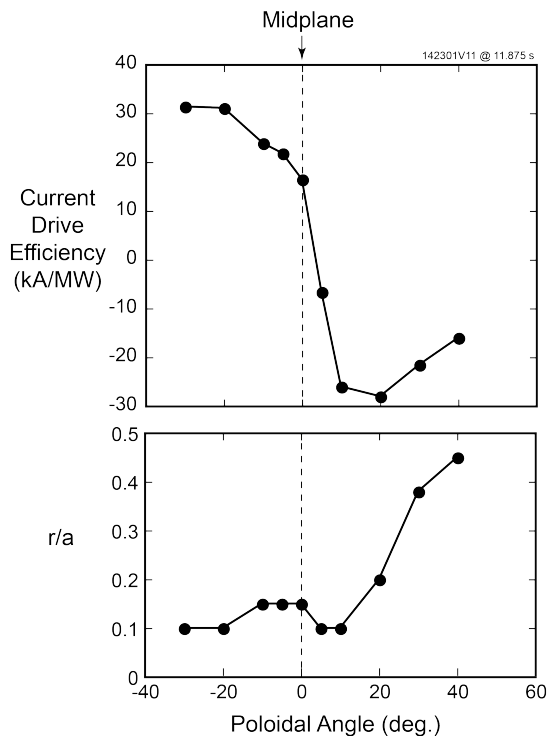


Figure 7.2.5: (a) EBW current drive efficiency versus poloidal angle of the mirror launcher. Negative angles correspond to the launcher being below the midplane and negative current drive efficiency is counter current drive. (b) Normalized minor radius where the peak driven current density is generated.

Modeling of the EBW heating and current drive assumed a launched $n_{\parallel} = \pm 0.7$. The EBW rays were launched at the LCFS and the vertical location of the launched rays was scanned above and below the midplane. Figure 7.2.5 summarizes the CQL3D current drive modeling results for 1 MW of EBW power. The maximum current drive efficiency is 30 kA/MW. When the launching mirror is 30 degrees below the midplane the current is driven in the co-current direction near the magnetic axis. When the launching mirror is 10 degrees or more above the midplane the current is driven in the counter current direction. As the mirror is moved even further above the midplane the EBW-driven current peaks further off axis. Launching the EBW power more than 30 degrees above the midplane resulted in large Doppler shifts, so that the EBW power was absorbed well off axis and the EBW power deposition profile became very broad.

The multi-megawatt O-X-B heating system will not be implemented during the period of this 5-year plan, even with 10% incremental funding. However, the antenna of the 1 MW, 28 GHz EC heating system discussed earlier can be modified to allow a test of O-X-B heating during the flat top of NSTX-U NBI H-mode discharges in Year 5.

7.2.2.6 Summary of Research Plan by Year for Thrust RF-1 **Assuming a Baseline Funding Scenario (*Baseline + 10% incremental scenario in italics*)**

Year 1 (FY2014):

- Complete simulation of 28 GHz heating system for non-inductive startup and complete conceptual system design.
- Continue simulation of 28 GHz EBW heating and current drive in NSTX-U advanced scenarios and begin conceptual design for O-X-B heating system.

Year 2:

- Generate a sustained fully non-inductive 300-500 kA H-mode discharge with FW power using an inductively generated target discharge.
- EBW emission data acquired to assess O-X-B coupling efficiency (see section 7.3.2).

Year 3:

- Non-inductively ramp I_p in a FW-only H-mode discharge from 300 to 500 kA. These experiments will benefit from current density measurements with the new motional Stark effect laser-induced fluorescence (MSE-LIF) diagnostic (see section 10.6.1.5) which uses a low-power, non-perturbing diagnostic neutral beam rather than the heating beam used by the conventional MSE collisionally-induced fluorescence, (MSE-CIF) diagnostic.
- Assess of the impact of FW heating on NBI current ramp-up. A combination of NBI and FW heating will be to non-inductively ramp-up the plasma current from 300-400 kA to 0.8-1 MA. These experiments will assess the impact of adding FW heating to the NBI heated current ramp-up. These experiments will be continued in Year 4.
- Continue acquiring EBW emission data to assess O-X-B coupling efficiency (see section 7.3.2).

Year 4:

- Continue to assess of the impact of FW heating on NBI current ramp-up.

Year 5:

- 28 GHz EC heating of a CHI plasma. Target conditions will be adjusted for maximum 28 GHz single pass absorption. Core heating with X-mode second harmonic EC heating at $B_T(0) \sim 0.5$ T and O-mode fundamental EC heating at $B_T(0) \sim 1$ T will be studied. TSC simulations predict 0.6 MW of second harmonic 28 GHz EC heating will increase $T_e(0)$ of the CHI target plasma from ~ 5 eV to ~ 400 eV in 20 ms. If reproducible EC-heated

CHI target plasmas can be generated with $T_e(0) \geq 100$ eV they will be heated with FW power to non-inductively ramp the plasma current.

- Non-inductive start-up with EBW heating. The grooved graphite mirror polarizer on the center stack that is needed for these experiments will be installed in NSTX-U during the Year 3-4 machine outage.
- Test 28 GHz EBW heating via O-X-B coupling with a fixed horn antenna. EBW emission data acquired in Year 2-3, together with numerical simulations for specific discharge scenarios, will be used to adjust the launch direction of the 28 GHz horn used for EC heating, so that it efficiently couples to EBWs in the plasma. Experiments would initially attempt core electron heating, because it is easier to detect. If these on-axis heating experiments prove successful, experiments would be extended to off-axis heating, and possibly current drive, if sufficient power can be coupled to the plasma. These experiments would provide valuable experimental data to verify predictions of numerical simulations of EBW heating by advanced RF codes.

7.2.3 Thrust RF-2: Validate Advanced RF Codes for NSTX-U and Predict RF Performance in Future Devices

7.2.3.1 Validate Advanced RF Codes that Include SOL, Realistic Antenna Geometry, Accurate Modeling of Fast-Ion Interaction and the Effect of Edge Fluctuations

An extensive suite of advanced RF simulation codes directly supports the RF experimental research program on NSTX-U, and the existing domestic plasma fusion research program in general. These codes are, and will be, used to predict RF heating and current drive performance in ITER and other fusion devices. A major NSTX-U RF research program goal is therefore to advance the development of these RF theory and simulation tools by experimentally testing their predictions for NSTX-U RF-heated plasmas. Many of these advanced RF numerical codes are currently being upgraded to include detailed models of the SOL and plasma edge region near the LCFS, including edge fluctuations that can scatter RF power, and in the case of AORSA-3D [10] a high-resolution model of the FW antenna. For modeling FW heating, inclusion of the SOL and edge enables the simulation of RF excited normal modes that may contribute to parasitic loss of injected RF power. To complement these upgrades to the advanced RF codes the diagnostics on NSTX-U will be improved to better measure RF fields and power flows, near the antenna, in the SOL and on the divertor plates. Also the edge and SOL reflectometer is being upgraded to operate over a larger frequency range in order to measure the density profile at the higher toroidal fields where NSTX-U will operate. In addition the reflectometer's data acquisition system is being upgraded to acquire more data at a higher rate than was possible on NSTX.

Several numerical codes have now been developed and upgraded to more accurately model the FW interaction with ions in discharges heated by a combination of FW and NBI power. These codes will be invaluable for predicting ICRF heating and current drive in ITER discharges. There will be several enhancements to NSTX-U diagnostics that can measure changes in the fast-ion distribution due to FW ion acceleration that will allow these code predictions of fast-ion behavior to be tested. Upgrades to the multi-point Thomson scattering and MSE diagnostics will also provide improved measurements of RF power deposition and the current density profile that can be compared to the predictions from numerical simulations.

During the period of this five-year plan, detailed diagnostic data from the new and upgraded diagnostic suite on NSTX-U will have been acquired during FW-only H-mode discharges and FW-heated NBI H-modes discharges. Also the advanced RF codes will have undergone significant upgrades to more realistically simulate both RF losses in the SOL and FW interaction with ions inside the LCFS. It will therefore be possible to conduct a detailed validation of these more realistic RF simulations.

7.2.3.2 Use of Advanced RF Codes to Predict RF Performance in ITER and Future Fusion Devices

The advanced RF numerical codes will be upgraded and modified in response to their validation against NSTX-U experimental data for a wide range of plasma regimes, including RF heating during plasma current start-up, ramp-up, and during NBI H-mode discharges. Once the codes have been shown to accurately simulate NSTX-U discharges in these regimes they will be used to predict RF performance in ITER and future fusion devices.

7.2.3.3 Summary of Research Plan by Year for Thrust RF-2 Assuming a Baseline Funding Scenario (*Baseline + 10% incremental scenario in italics*)

Year 1 (FY2014):

- Upgrade advanced RF codes to include SOL, realistic antenna geometry, accurate modeling of fast-ion interactions and effect of edge fluctuations.

Year 2-3:

- Detailed validation of advanced RF codes that include accurate SOL and antenna modeling using data from the upgraded diagnostic suite on NSTX-U for H-mode scenarios that employ FW heating and current drive.

Year 4-5:

- Use advanced RF codes to predict RF performance in ITER and future fusion devices.

7.3 Timelines for Tool Development Needed to Achieve Research Goals

7.3.1 Theory and Simulation Capabilities

As a national facility, the development of RF theory and simulation capabilities on NSTX-U involves a collaborative effort between the PPPL NSTX-U physicists and their counterparts in the Alcator C-Mod and DIII-D programs, as well as significant support from the USDOE CSWPI. The funding support includes direct support from the NSTX-U project, individual grants and contracts from USDOE to various institutions such as the PSFC-MIT and CompX, as well as support through the RF-SciDAC Center. Understanding the underlying physics of the RF heating, current drive, interactions with fast-ion populations, and the coupling of power to the plasma and translating that understanding into validated simulation codes that include physics details over a wide range of parameters is a common need for all of these programs. In the following sections details of specific RF numerical simulation codes that support the NSTX-U 5-year wave heating and current drive research plan are discussed.

7.3.1.1 AORSA Full-Wave Code

In its present form, the All Orders Spectral Algorithm (AORSA) full-wave tool [15] lacks a high-fidelity, geometry-accurate antenna model, any slow-wave propagation in the SOL (due to

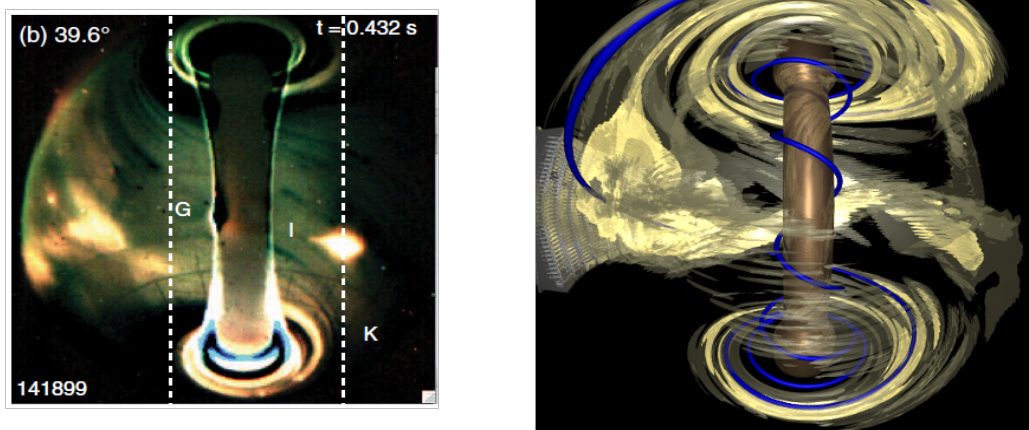


Figure 7.3.1: The left panel shows a visible light image indicating the edge RF power flow following magnetic field lines from the antenna to the divertor during an FW-heated NBI H-mode discharge in NSTX. The right panel shows the AORSA-3D simulation results for the electric wave field magnitude for this case.

resolution constraints), and is typically run with SOL density profiles that are simplified and/or approximate due to the lack of available constraining observations. During the first two years of the 5-year plan these capabilities will be added to AORSA. The impact of any edge localized RF excited normal modes that contribute to parasitic loss of RF power will then be evaluated. Although preliminary work in this area suggests that the Poynting flux associated with FW excited RF normal modes of the SOL is not correlated with that observed in the optical camera images obtained on NSTX during FW heating of NBI H-mode discharges (Fig. 7.1.3(a) and Fig. 7.3.1), a further study will be conducted to examine tracer particles in the FW electric wave-fields calculated by AORSA-3D to investigate if there is a field-aligned particle flux that is accelerated either by the SOL RF normal modes, or the near field of the FW antenna. Normal modes localized near the LCFS have been seen in AORSA results for negative toroidal mode numbers [25], and these modes do exhibit field-aligned Poynting flux, but at the LCFS, not in the SOL as seen in NSTX (c.f., Fig. 7.1.3(a) and Fig. 7.3.1). Long-range plans are to couple AORSA to a high-fidelity antenna model (e.g., VORPAL [26]) that includes a self-consistent RF sheath with AORSA-3D. Such a coupling will provide an electric wave-field solution suitable for examining stochastic heating that may be another possible cause for the observed field-aligned power flow.

EBW heating schemes depend on mode conversion, either via tunneling between the fast X-mode and the EBW (X-B) or via double mode conversion from the O-mode to slow X-mode to the EBW (O-X-B). As such assessing these heating schemes requires some estimate of how much power is converted from the launched mode, to the EBW mode. These conversion efficiencies are typically estimated using 0-D expressions that ignore any effects due to density fluctuations and turbulence in the edge and SOL plasma. However, according to [27] an observed 30% variation in transmission/emission efficiency is probably due to density fluctuations in the plasma edge. AORSA-1D will be used to map the transmission/emission coefficients for the k-space spectrum of a launched wave for arbitrary density profiles, e.g., turbulent density data from a transport simulation. These results will be compared with the standard transmission formulas used in ray tracing calculations (c.f. ref [28] and references therein). The aim will be to predict any degradation in heating efficiency associated with density fluctuations.

7.3.1.2 TORIC full Wave Code, with SOL Model

The present edge model in the TORIC solver [16] consists of a SOL that extends out to a Faraday screen and beyond that is a current strap in vacuum. A conducting wall is placed in the back of the current strap. The locations of the current strap, Faraday screen, and conducting wall correspond to conforming flux surfaces and their locations can be specified arbitrarily. Similarly, the density profile and width of the SOL are also arbitrary. The caveats are that the magnetic

equilibrium in the vacuum region is taken to be closed flux surfaces and the SOL width is imposed using the region just inside the LCFS so that the effective minor radius of the plasma is reduced slightly. Initially this simplified SOL model in TORIC will be used to perform simulations with the Faraday screen removed and the current strap placed right at the edge of the plasma SOL, with a vacuum region extending from the outside edge of the current strap to the conducting wall. Surface wave excitation will then be studied in a manner similar to what has been done with the AORSA solver, whereby 3-D field reconstructions are done by calculating the 2-D (ψ , θ) electric field solutions with TORIC for each toroidal mode of the antenna and then superposing these solutions. Over the longer term the plan is to take advantage of work being carried out with TORIC in the CSWPI where the core solver will be combined with an edge model such as the VORPAL code [28], which allows realistic treatment of the 3-D solid geometry of the ICRF antenna structure and vacuum vessel. This coupling will be done either through standard admittance matrix techniques or through more direct methods that rely on finding regions of overlap between the boundary and core solutions.

7.3.1.3 GENRAY Ray Tracing and TORBEAM Beam Tracing Codes

GENRAY is a ray tracing code based on the geometrical optics approximation for the calculation of electromagnetic wave propagation and absorption in tokamak plasma geometry [17]. While the beam tracing code TORBEAM [29], which is based on the paraxial WKB approximation, takes into account diffraction effects in the RF beam propagation. GENRAY includes a current drive calculation, ADJ [30] that uses an adjoint approach based on the Coulomb Fokker-Planck collisional operator and the relativistic quasilinear flux. GENRAY has been generalized recently to include a 2-D model for the SOL [31] and the effects of scattering induced by edge density fluctuations in the lower hybrid frequency regime [32]. Following the approach in [33], this scattering model utilizes a wave kinetic equation, which is solved by a Monte-Carlo technique. An extension of this scattering model for the FW regime will be implemented in GENRAY in order to evaluate the possible role of scattering in NSTX-U plasmas. GENRAY will also be generalized for the EBW/EC frequency regime in order to evaluate the importance of scattering in NSTX-U plasmas, taking into account several important features already present in the GENRAY code, such as the calculation of the critical angle for EBW O-X-B mode conversion (which depends strongly on the edge density gradient) and the estimate of the reduced coupling if waves are launched away from the optimum angle for O-X-B coupling. An accurate validation of GENRAY and TORBEAM for NSTX-U plasmas will be performed. Such numerical analysis will be also used to predict RF heating performance in future fusion devices.

7.3.1.4 CQL3D Fokker-Planck Code

The CQL3D bounce-averaged Fokker-Planck finite-difference code [18, 19] has been used successfully for modeling the NBI and FW heating in NSTX, particularly including the quasi-

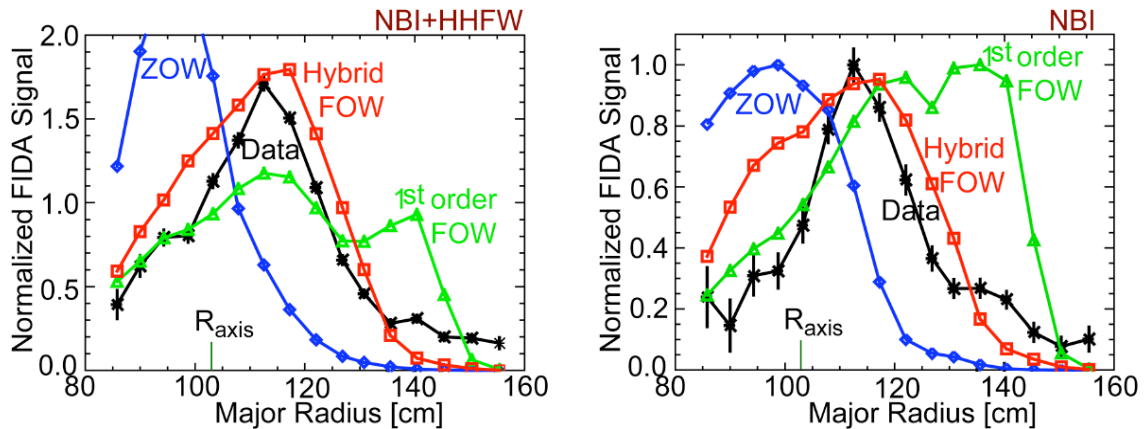


Figure 7.3.2. Experimental FIDA diagnostic fast-ion radial profiles compared to the original zero-orbit-width (ZOW) results from CQL3D, the 1st order finite-orbit-width (FOW) results, and the much more accurate hybrid-FOW results. Calculated FIDA results are normalized to the NBI experimental data. The same normalization is used for the NBI+FW modeling, after reducing FW nominal input power by 35% to account for RF edge losses.

linear RF wave-interaction [34-36]. Along with the GENRAY ray tracing code model for FW, a strong interaction with the NBI ions is obtained [34]. Finite-orbit-width (FOW) effects have recently been implemented in the code [37], computing the bounce-averaged Fokker-Planck terms along guiding-center ion orbits. Two different versions are being developed: (1) A Hybrid-FOW model in which partial FOW capabilities are implemented, namely in the formation of the NBI source, the RF quasi-linear diffusion operator, the particle diagnostics, and the loss cone. There is no neoclassical radial transport in this version. The main advantage of this version of the code is that it is as fast as the original zero-orbit-width (ZOW) version. Initial applications show a marked improvement in the description of diagnostic signals in NSTX, as shown in Fig 7.3.2 [37].

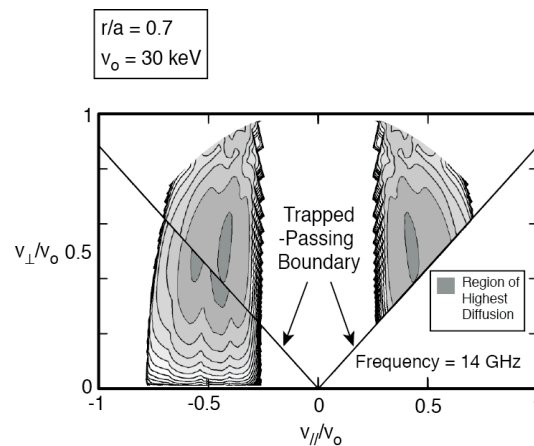


Figure 7.3.3: Contours indicating the strength of the quasi-linear diffusion operator due to the RF $[u^2 D_m]$ versus the perpendicular and parallel velocity, normalized to $v_o = 30$ keV, at the peak of the EBW power deposition profile located at $r/a = 0.7$ for 1 MW of 14 GHz power launched into the $\beta = 42\%$ NSTX plasma. The quasi-linear diffusion peaks near the trapped-passing boundary. (From ref. [1])

(2) A full-FOW neoclassical model including radial transport and non-thermal bootstrap current is currently under development. An intermediate first order orbit shift model was also developed for application to NSTX, but the fast-ion orbits were too large for this approximation, as shown in Fig. 7.3.2.

Recently the FW quasi-linear coefficients calculated by the AORSA full-wave code [38] have been coupled to CQL3D. Additional wave-particle physics will be included with the Diffusion Coefficient (DC) code, as described in the following section 7.3.1.5.

The CQL3D code applied to electrons has enabled calculation of EBW absorption and current drive in the NSTX tokamak [1, 39]. Figure 7.3.3 shows the strength of the quasi-linear diffusion operator across the trapped-passing boundary due to RF in an NSTX discharge with EBW heating (from ref. [1]). Similar scoping work and analysis will be carried out for NSTX-U [40]. EBW ray tracing from GENRAY provides the data necessary for CQL3D to calculate the RF quasi-linear coefficients. Iteration between EBW absorption giving the EBW electric field strength, and the solution of the Fokker-Planck equation for the non-thermal electron distributions on which the absorption depends, provides self-consistent distributions and absorption profiles. Current drive is calculated from the non-thermal distributions. Off-axis current drive efficiencies were obtained [1] which are about twice that calculated and measured for ECCD near the axis in the DIII-D tokamak. This was determined to be largely due to Ohkawa current drive [41] resulting from a property of EBWs that gives enhanced quasi-linear velocity diffusion near the trapped-passing boundary, rather than the more usual Fisch-Boozer current drive [42].

7.3.1.5 Diffusion Coefficient (DC) Code

The DC code calculates “exact” full-wave RF diffusion coefficients by numerically integrating

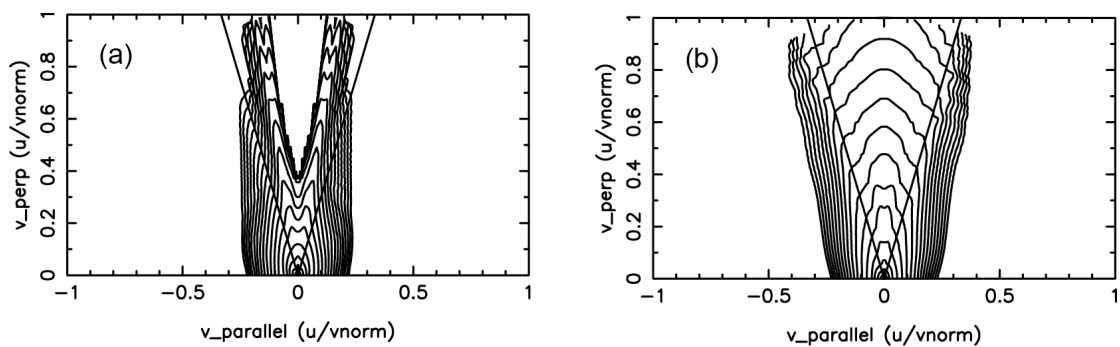


Figure 7.3.4: Contours of minority H^+ ion distributions at $\rho/a=0.143$ for 10 msec after beginning of the ICRF simulations. (a) Results from AORSA quasi-linear coefficients, and (b) from the Lorentz-orbit based DC diffusion coefficients. Velocity normalization corresponds to 5 MeV. Contour levels are chosen to be equal spaced for the initial Maxwellian distribution.

the Lorentz force equation for the gyro-orbits of ions in computational equilibria derived from magnetic field data plus the AORSA [15] or TORIC [16] full-wave electromagnetic fields. This provides a means for examining the impact of FOW, finite Larmor radius, correlation and nonlinear effects on ICRF ion diffusion. The particles are launched from mid-plane points in the tokamak, initially equal spaced in gyro-phase (with constant gyro-radius) about the given gyro-centers and also equal spaced in toroidal length along a given RF mode wavelength, and averages the resulting square of the velocity changes after one (or more) poloidal circuits, to obtain the ICRF bounce-averaged, gyro-phase and wave-phase averaged diffusion tensor. This is carried out for a 3-D array (u_{\parallel} , u_{\perp} , R) of initial conditions, giving the six independent RF diffusion coefficients in 3-D constant-of-motion space. The method follows the formalism of Refs. [43, 44]. FW heating in NSTX-U will allow examination of the effects of wave-induced radial pinch and diffusive transport, in addition to harmonic overlap and correlation effects on velocity space diffusion. Figure 7.3.4 compares the calculated ion distribution function in a Alcator C-Mod ICRF heating simulation using (a) diffusion coefficients obtained from AORSA [15] using quasi-linear theory, and (b) velocity space diffusion coefficients from Lorentz-orbit DC calculations. The resulting heating profiles were close in both cases, but the differences in the tail distributions can strongly affect relevant tail ion diagnostics.

7.3.1.6 AORSA/ORBIT-RF Full-Wave/Monte-Carlo Code

The 5-D finite-orbit Monte-Carlo code ORBIT-RF [45] coupled with the 2-D linear full wave

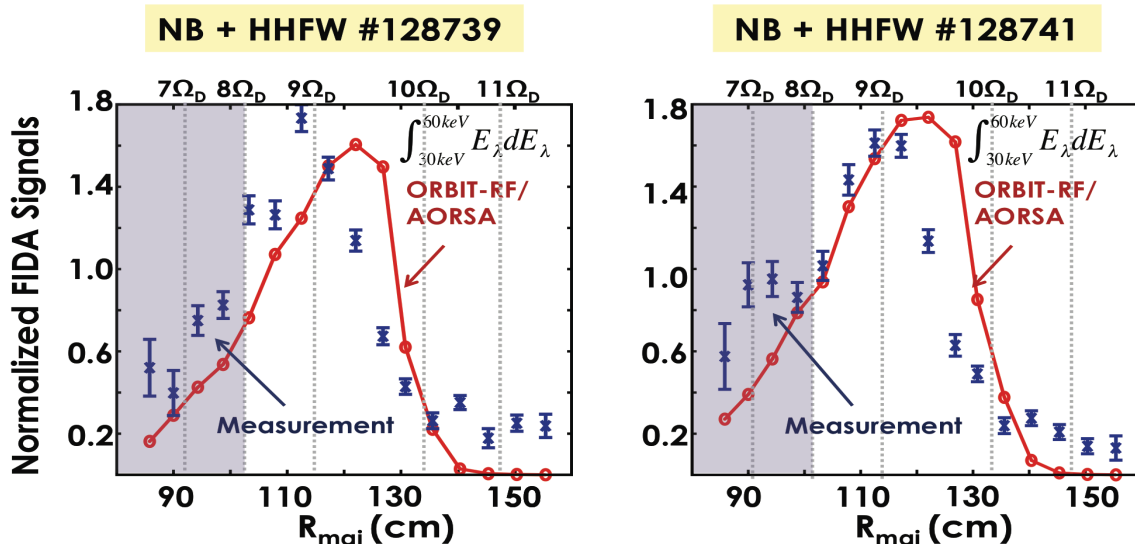


Figure 7.3.5: Comparison of enhanced synthetic FIDA signals from ORBIT-RF/AORSA (solid red lines) and the measured FIDA signal (blue points with error bars) for the two NSTX FW + NBI discharges (a) #128739 and (b) #128741. The beam injection power is 1 MW with a full energy of 65 keV.. 1 MW FW power is launched into the plasma at a frequency of 30 MHz.

code AORSA [46] is a comprehensive numerical model that can perform a fully self-consistent calculation of resonant interactions of injected beam ions with either a single FW or multiple FWs in the plasma. To validate the ORBIT-RF/AORSA simulation suite FIDA experimental fast-ion data were simulated for NSTX discharges heated by a combination of FW and NBI power. Computed beam ion distributions without and with 30 MHz FW were passed to the synthetic diagnostic simulation code FIDASIM [47]. Synthetic FIDA signals were computed for the two cases. For a more quantitative comparison of beam ion populations accelerated by FW, the enhancement was computed by taking the ratio of FIDA signals with and without FW (that is with NBI alone) in both the measurements and the simulations. In Fig. 7.3.5, computed enhancements are compared with measured enhancements for the two FW-NBI discharges (shots 128739 and 128741). Here, the beam ion energy was integrated in the energy range from 30 keV to 60 keV for comparison. ORBIT-RF/AORSA quantitatively reproduced the FIDA measurements for the two NSTX FW plus NBI discharges. However ORBIT-RF/AORSA computed slightly enhanced outboard radial shifts compared to the measurements.

For the initial 2 years of NSTX-U 5-year plan, ORBIT-RF/AORSA will be used to simulate a wide range of FW-NBI experiments to understand the conditions under which fast-ions are effectively accelerated by FW. ORBIT-RF is currently being coupled with TORIC. In addition to benchmarking ORBIT-RF/TORIC with ORBIT-RF/AORSA, both approaches will be tested against experimental data to ascertain the fidelity of each approach. For years 3-5 the two suites, ORBIT-RF/AORSA and ORBIT-RF/TORIC, will be compared with predictions from CQL3D/AORSA, CQL3D/TORIC and SPIRAL/TORIC (see section 7.3.1.7) which model the wave-particle interaction with a different formulation.

7.3.1.7 SPIRAL Using Fields from TORIC

The full Lorentz-orbit following code SPIRAL [48] has been modified to use the FW fields as calculated by the TORIC code. Ensembles of energetic ions can now be followed in the SPIRAL code in the presence of FW wave fields as calculated by the TORIC code. As a result the full interaction between the gyro-motion of the particles and the RF fields is included without any approximations. In the current version of TORIC a Maxwellian fast-ion distribution is assumed which is a poor approximation for the beam-ion slowing down distributions present in NSTX and NSTX-U. Work is under way to include non-Maxwellian distributions in TORIC and once implemented, an iterative method between TORIC and SPIRAL will be used to accurately calculate the interaction between the beam-ions and the FW power, and to compare these results with various measurements of the fast-ions, including confined and lost ion signals, and neutron signals.

7.3.1.8 Upgrade of NUBEAM with an RF Operator for FW

The presence of a fast-ion population in a discharge has a significant impact on FW power absorption. Several quasi-linear code couplings exist to account for both the non-Maxwellian fast-ion distributions, and to capture the self-consistency required between the launched FWs and the plasma ion distribution. This self-consistency typically involves a full-wave RF solver, and an update to the plasma distribution with an RF operator, usually a continuum Fokker-Planck or particle-based Monte-Carlo code. Of the available update codes, NUBEAM has the most comprehensive content in its physics operator, with the exception of an accurate RF operator. Recently PPPL and ORNL have restarted work to complete the inclusion of an RF operator in NUBEAM and the TRANSP framework [49].

In Year 1-2, following the completion of the RF operator in NUBEAM, the goal will be to accurately determine the power partitioning to the beam ion population, and contrast this with that seen using an assumed Maxwellian beam of equivalent temperature as is often done [50]. The impact of any finite-ion-orbit effects will also be examined by comparing coupled AORSA-NUBEAM quasi-linear self-consistent simulation results with experimental observations from the FIDA diagnostic.

7.3.2 Diagnostics and Other Facility Upgrades Supporting Wave Heating and Current Drive Research

This section provides a brief summary of some of the diagnostics systems and facility upgrades that will directly support the wave heating and current drive program on NSTX-U. More information regarding the status and plans for the RF heating and current drive systems and diagnostics systems on NSTX-U can be found in Sections 10.4 and 10.6, respectively.

The two IR cameras on NSTX proved to be invaluable in establishing that the “hot” RF produced spiral deposition patterns were caused by RF power flow along the magnetic field lines from the SOL in front of the antenna to the divertor floor/ceiling [9, 51, 52]. Two additional IR cameras will be installed on NSTX-U allowing a better characterization of this power flow and the toroidal heat deposition. The probe sets in divertor tiles will be augmented to include probes that have direct RF detection capability. Langmuir probes will provide measurements of the RF voltage across the probe sheath and allow the FW field strength at the “hot” RF-produced spiral deposition zones [51, 52] to be measured. RF loop probes will provide measurements of RF magnetic field strength and RF-induced currents in the vicinity of the RF-produced spirals. Probes in both the floor and ceiling will help to determine the directionality of wave excitation and separate direct propagation effects from standing wave effects. Magnetic and Langmuir RF probes installed in the tiles above and below the antenna will allow the measurement of the relative strengths of the RF fields propagating in both directions along the magnetic field lines.

The experimental characterization of FW effects on fast-ions from NB injection in NSTX-U requires accurate measurements of the fast-ion radial profile to identify the regions that mostly contribute to the wave-particle interaction process. In addition, information on the fast-ion response to RF waves in terms of energy and pitch will be needed to discern the behavior of different classes of particles, for example passing or trapped particles. Several diagnostics will provide complementary information on fast-ion interaction with FW power in NSTX-U. Two FIDA systems [53] will provide time, space and energy resolved measurements of the fast-ion distribution; a vertical FIDA system [54] more sensitive to trapped or barely co-going particles and a tangential FIDA system [24] that measures co-passing fast-ions. FIDA measurements will be complemented by an upgraded solid-state Neutral Particle Analyzer [55] array (ssNPA) that measures trapped fast-ions. Additional measurements that are helpful to study fast-ion interactions with FW will be provided by neutron rate counters, a new charged fusion product profile diagnostic [56] (CFPD) that is currently being tested on MAST and may possibly be available on NSTX-U, and a scintillator-based Fast Lost Ion probe [57] (sFLIP).

An upgraded 10-40 GHz reflectometer will provide measurements of plasma electron density profiles in front of the FW antenna array. These profiles will be utilized for RF coupling studies, including the assessment of antenna modifications and the effectiveness of lithium conditioning, gas puffing, and cryo-pumping to modify the SOL density and to mitigate FW losses in the SOL. The reflectometer will also be used to monitor power losses due to PDI, and for the measurement of localized electron density fluctuations in front of the FW antenna.

On NSTX-U there will be a new MSE-LIF diagnostic [58, 59] to measure the current density profile that requires only a low-power, 30-40 kV, 30 mA diagnostic beam blips, in addition to the “conventional” MSE-CIF diagnostic previously used on NSTX [60] that requires a high-power heating beam. Because the MSE-LIF diagnostic uses a non-perturbing, low-power diagnostic neutral beam it is much better suited to measuring the plasma current density profile in plasmas that have no high-power NBI heating; for example during RF-driven, non-inductive plasma current ramp-up experiments.

A 28 GHz, megawatt power level, EC/EBW heating system is planned for installation on NSTX-U. Assuming a baseline NSTX-U budget this system will become operational in Year 4. Initially this system will provide electron heating during non-inductive plasma start-up, later it will be used for off-axis EBW heating and current drive. The EC/EBW heating system will use a 28 GHz, 1 MW gyrotron originally developed for EC heating in the GAMMA-10 tandem mirror [61]. The gyrotron will be powered by a modified TFTR NBI power supply that will be capable of powering several megawatt-level gyrotrons. The plasma start-up system will use an HE-II low-loss corrugated waveguide and fixed horn antenna.

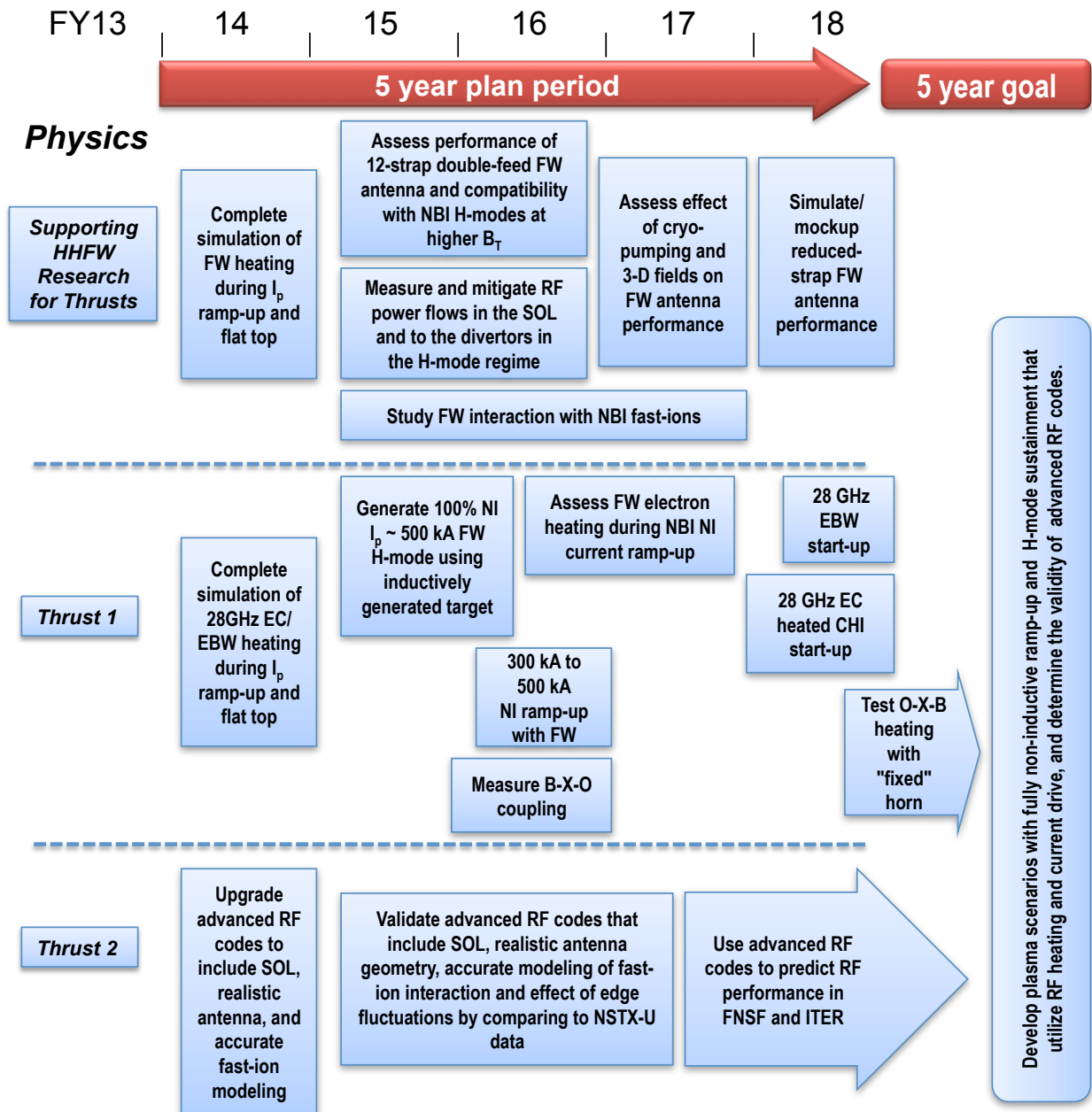
The York Plasma Institute at the University of York in the United Kingdom has proposed a collaboration with NSTX-U that involves the installation of a Synthetic Aperture Microwave Imaging diagnostic (SAMI) [62] in Years 2-3. Amongst other things, the SAMI diagnostic will measure the B-X-O mode conversion efficiency and determine where the conversion efficiency is a maximum and how stable the angular mode conversion window is with respect to fluctuations in the edge and/or core. These EBW mode conversion measurements will provide valuable data for designing an off-axis EBW heating & current drive system for NSTX-U in Year 4 and for initial tests of O-X-B heating used the fixed horn antenna in Year 5.

References

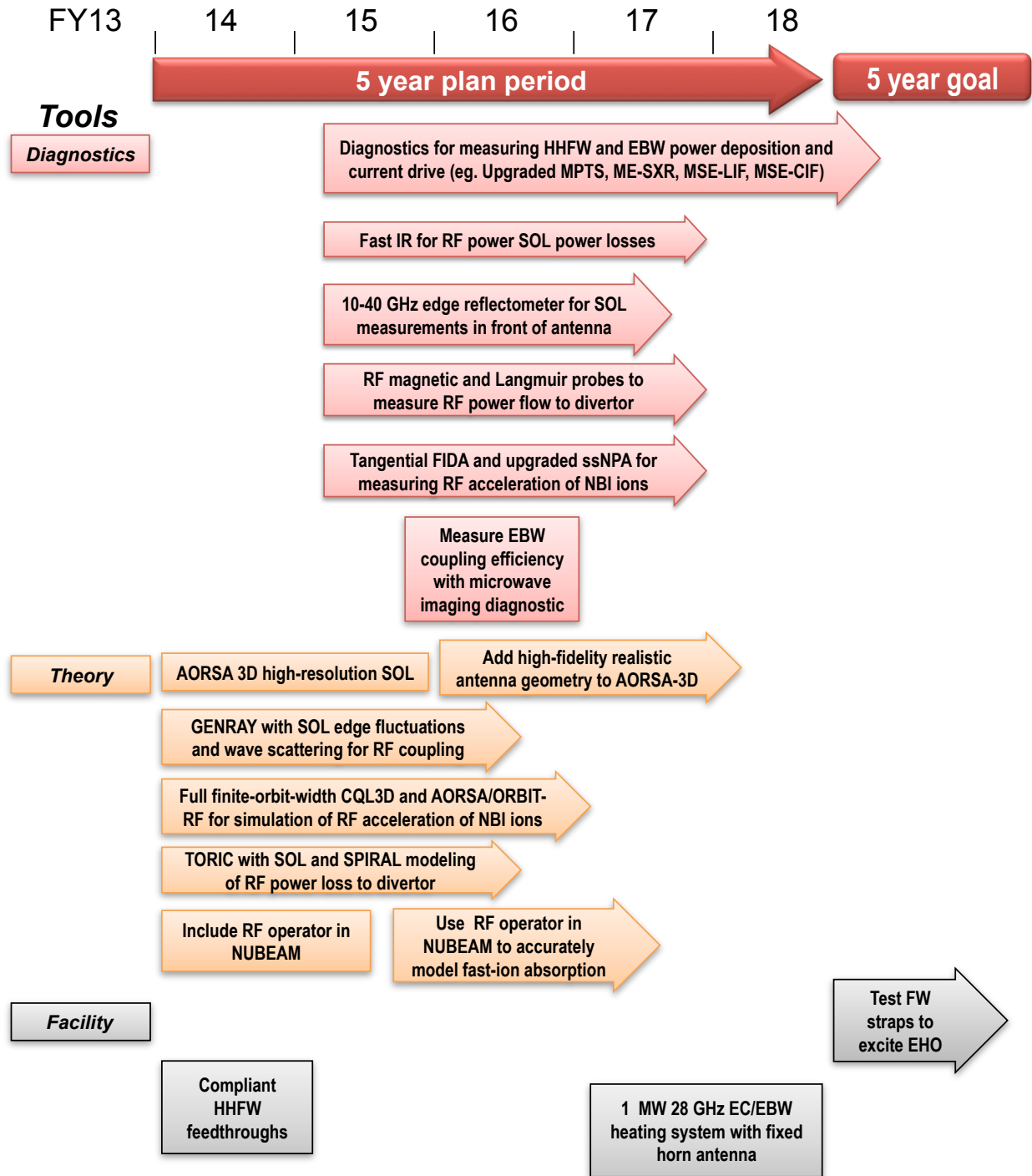
- [1] G. Taylor et al., Phys. Plasmas **11** (2004) 4733-4739.
- [2] J. Urban et al., Nucl. Fusion **51** (2011) 083050.
- [3] J. R. Wilson et al., Phys. Plasmas, **10** (2003) 1733-1738.
- [4] J. C. Hosea et al., Phys. Plasmas **15** (2008) 056104.
- [5] C. K. Phillips et al., Nucl. Fusion **49** (2009) 075015.
- [6] J. C. Hosea et al., AIP Conf Proceedings **1187** (2009) 105-112.
- [7] G. Taylor et al., Phys. Plasmas **17** (2010) 056114.
- [8] J. C. Hosea et al., AIP Conf. Proceedings **1406** (2011) 333-336.
- [9] R. J. Perkins et al., Phys. Rev. Lett. **109** (2012) 045001.
- [10] D. L. Green et al., Phys. Rev. Lett. **107** (2011) 145001.
- [11] G. Taylor et al., Phys. Plasmas **19** (2012) 042501.
- [12] S. J. Diem et al., Phys. Rev. Lett. **103** (2009) 015002.
- [13] S. J. Diem et al., Nucl. Fusion **49** (2009) 095027.
- [14] V. F. Shevchenko et al., Nucl. Fusion **50** (2010) 022004.
- [15] E. F. Jaeger et al., Nucl. Fusion **46** (2006) S397-S408.
- [16] M. Brambilla, Plasma Phys. and Cont. Fus. **44** (2002) 2423-2443.
- [17] A. P. Smirnov and R. W. Harvey, Bull. Am. Phys. Soc. **40** (1995) 1837.
<http://www.compxco.com/genray.html>
- [18] R. W. Harvey and M.G. McCoy, The CQL3D Code, *Proc. IAEA TCM on Advances in Simulation and Modeling of Thermonuclear Plasmas*, pp. 489-526, Montreal, (1992), USDOC/NTIS No. DE93002962; <http://www.compxco.com/cql3d.html> .
- [19] R. W. Harvey et al., Proc. 38th EPS Conf. on Plasma Phys. (Strasbourg, France 2011) paper P4.017 <http://www-fusion-magnetique.cea.fr/eps2011/> .
- [20] P. M. Ryan et al, AIP Conf. Proc. **1406** (2011) 101-104.
- [21] B. P. LeBlanc et al., IAEA, Daejeon, Republic of Korea (2010), paper EXW/P7-12.
- [22] TRANSP group, PPPL, <http://w3.pppl.gov/transp/>
- [23] B. P. LeBlanc et al., AIP Conf. Proc. **1187** (2009) 117-120.
- [24] A. Bortolon et al., Rev. Sci. Instrum. **81** (2010) 10D728.
- [25] D. L. Green et al., AIP Conf. Proc. **1406** (2011) 337-340.
- [26] D. Smithe, et al., “*Self-consistent modeling of the tokamak RF antennas, edge plasma, and sheath voltages*”, APS-DPP, (2012) Paper TP8.00070.
- [27] G. Taylor et al., Phys. of Plasmas **12** (2005) 052511.
- [28] A.K. Ram and S.D. Schultz, Phys. Plasmas **7** (2000) 4084-4094.
- [29] E. Poli et al., Comput. Phys. Commun. **136** (2001) 90-104.
- [30] A. P. Smirnov et al., Proc 15th Workshop on ECE and ECRH (World Scientific 2009) pp. 301-306
- [31] G. M. Wallace et al. Phys. Plasmas **17** (2010) 082508.

- [32] N. Bertelli et al., “*The Effects of the Scattering by Edge Plasma Density Fluctuations on Lower Hybrid Wave Propagation*” submitted to Plasma Phys. Control. Fusion (2012).
- [33] P. T. Bonoli and E. Ott., Phys. Fluids **25** (1982) 359-375.
- [34] A. L. Rosenberg et al., Phys. Plasmas **11** (2004) 2441-2452.
- [35] D. Liu et al., Plasma Phys. Cont. Fus. **52** (2010) 025006.
- [36] R. W. Harvey et al., “Temporal Dynamics of NSTX NBI+FW Discharges using CQL3D-Hybrid-FOW” Bull. Am. Phys. Soc. 57 (2012) Paper PP8.00020.
- [37] Yu.V. Petrov and R.W. Harvey, “*Finite Orbit Width Features in the CQL3D Code*”, paper TH/P6-02, IAEA FEC, San Diego, CA (2012).
- [38] E. F. Jaeger, et al., Phys. Plasmas **15** (2008) 072513.
- [39] R. W. Harvey and G. Taylor, Phys. of Plasmas **12** (2005) 052509.
- [40] G. Taylor et al., Proc. 17th Workshop on ECE and ECRH, EPJ Web of Conferences **32** (2012) 02014 <http://www.epj-conferences.org/>
- [41] T. Ohkawa, National Technical Information Service Report No. PB2000-108008, (1976) [T. Ohkawa, General Atomics Report No. GA-A13847 (1976) (unpublished).]
- [42] N. J. Fisch and A. Boozer, Phys. Rev. Lett. **45** (1980) 720-722.
- [43] A. Kaufman, Phys. Fluids **15** (1972) 1063-1069.
- [44] L-G. Eriksson and P. Helander, Phys. Plasmas **1**,(1994) 308-314.
- [45] M. Choi et al., Phys. Plasmas **16** (2009) 052513.
- [46] D. L. Green et al., AIP Conf. Proc., **1187** (2009) 569-576.
- [47] W. W. Heidbrink et al., Comp. Physics **10** (2011) 716-741.
- [48] G. J. Kramer, et al., Plasma Phys. Cont. Fus. **55** (2013) 025013
- [49] B. H. Park et al., “*Status of RF heating model in NUBEAM*”, APS-DPP (2012) Paper JP8.00122.
- [50] R. I. Pinsky, et al., Nucl. Fusion **46** (2006) S416-S424.
- [51] R. J. Perkins et al., Proc. 39th EPS Conf. on Plasma Physics 36F (Stockholm, Sweden 2012) paper P-1.011
- [52] R. J. Perkins et al., Proc. 24th IAEA Fusion Energy Conference (San Diego, California 2012) paper EX/P5-40
- [53] W. W. Heidbrink, Rev. Sci. Instrum. **81** (2010) 10D727.
- [54] M. Podestà et al., Rev. Sci. Instrum. **79** (2008) 10E521.
- [55] D. Liu et al., Rev. Sci. Instrum. **77** (2006) 10F113.
- [56] W. U. Boeglin et al., Rev. Sci. Instrum. **81** (2010) 10D301.
- [57] D. S. Darrow, Rev. Sci. Instrum. **79** (2008) 023502.
- [58] E. L. Foley and F. M. Levinton, Rev. Sci. Instrum. **77** (2006) 10F311.
- [59] E. L. Foley and F. M. Levinton, *J. Phys. Conf. Ser.* **227** (2010) 012007.
- [60] F. M. Levinton and H. Yuh, Rev. Sci. Instrum. **79** (2008) 10F522.
- [61] T. Kariya et al, J. Infrared, Millimetre and Terahertz Waves **32** (2011) 295-310.
- [62] S. Freethy et al., Proc. 38th EPS Conference on Plasma Physics (Strasbourg, France, 2011) paper P2.050 <http://ocs.ciemat.es/EPS2011PAP/html/>

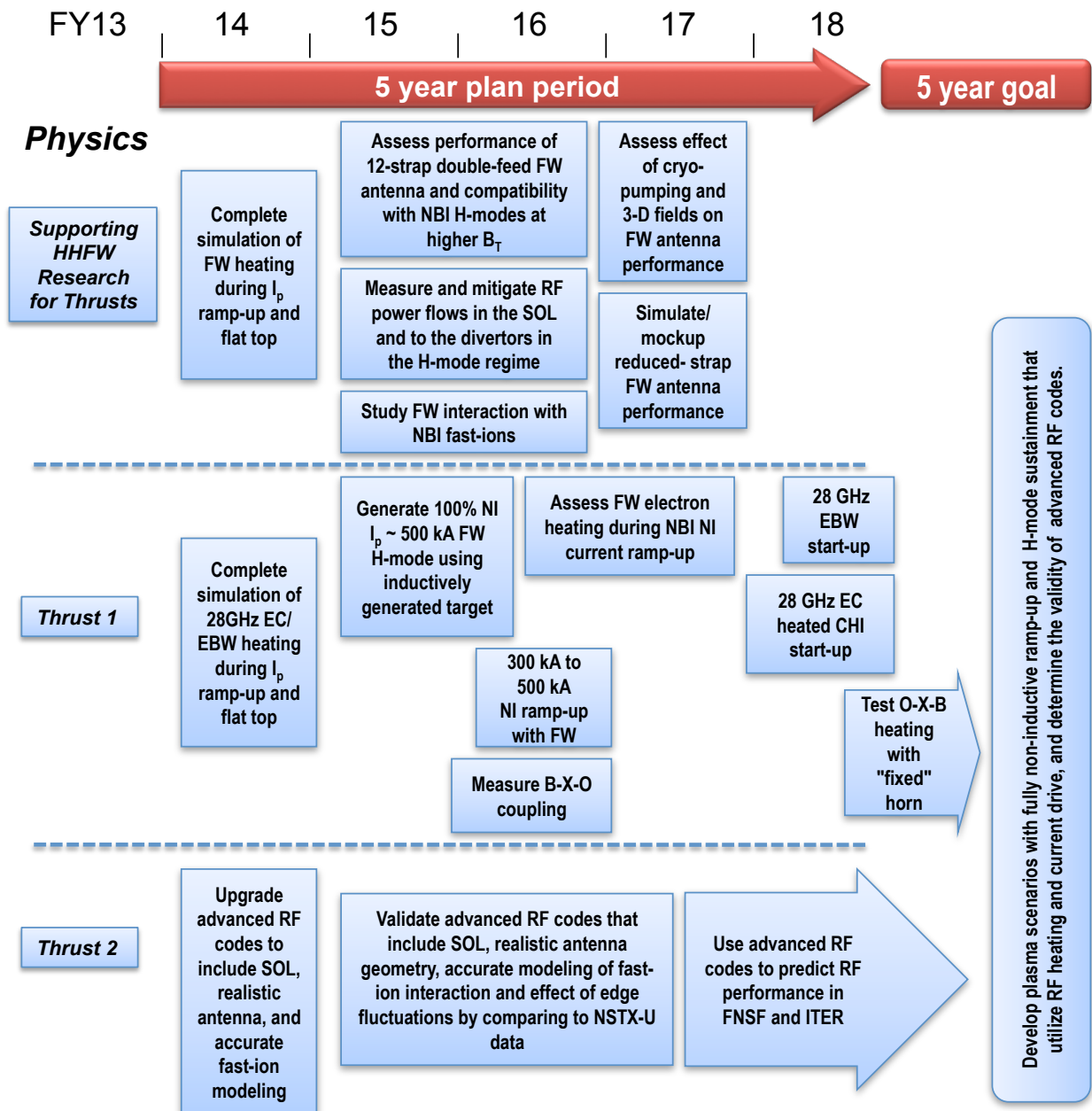
2014-18 Waves Heating and Current Drive Research Timeline (Assuming Baseline Funding)



2014-18 Waves Heating and Current Drive Research Timeline (Assuming Baseline Funding)



2014-18 Waves Heating and Current Drive Research Timeline (Assuming Baseline + 10% Funding)



2014-18 Waves Heating and Current Drive Research Timeline (Assuming Baseline + 10% Funding)

